^{228}Ra and ^{226}Ra radioactivities of the surface water in the northwestern North Pacific

1. Introduction

In the northwestern North Pacific, two western boundary currents, the Kuroshio and the Oyashio, are associated with the subtropical anticyclonic and subarctic cyclonic gyres, respectively. These currents interact with each other, resulting in a system known as the Kuroshio-Oyashio boundary region, which is characterized by a complex frontal structure and mixing of water masses (Kawai, 1972). To the north of this region, the Western Subarctic Gyre flows southwestward from the Bering Sea (Fig. 1). A part of the Western Subarctic Gyre flows into the Okhotsk Sea through the northern Kuril Straits (e.g. Ohtani, 1989). The Okhotsk Sea Water outflows to the Pacific through Bussol Strait, where it mixes with the Western Subarctic Gyre to form the Oyashio (e.g. Yasuda, 2003). The Oyashio moves south along the southeastern coast of Hokkaido and merges with the Tsugaru Current off Honshu, which then flows out of the Japan Sea into the Pacific through the Tsugaru Strait (between Hokkaido and Honshu) (e.g. Yasuda et al., 1988). The Kuroshio is the western boundary current of the North Pacific subtropical gyre and flows northeastward along Honshu. Water that comprises the Subtropical Water in the south of the Kuroshio, consists of warm and highly saline water. Despite the considerable structural complexity of water masses in the northwestern North Pacific, except for physical oceanography, relatively few studies have been conducted in the area to date.

Radium isotopes, ^{228}Ra and ^{226}Ra, are naturally occurring radionuclides that have been used extensively as tracers for seawater mixing due to their soluble nature (e.g. Nozaki et al., 1990). ^{228}Ra (half-life of 5.75y) is used in such studies, especially for studying areas close to continents and the ocean bottom (Moore et al., 1986; Rutgers van der Loeff et al., 1995 and 2003; Kadko and Muench, 2005; Nakano-Ohta and Sato, 2006),

the transport of particulate matter in the water column (Legeleux and Reyss, 1996; van Beek et al., 2007), and the vertical flux of nutrients in the upper ocean (Ku et al., 1995; Nozaki and Yamamoto, 2001; Cai et al., 2002). Since ^{228}Ra is produced by the decay of ^{232}Th, which is concentrated in sediments and soil, the isotope is provided to the seawater from river water and from sediments at the continental shelf. The concentration of ^{228}Ra in surface seawater decreases in the course of mixing with open ocean water and because of radioactive decay. ^{226}Ra is also produced from Th isotope (^{230}Th) enriched in bottom sediment. However, because of its longer half-life (1,600y), the concentration gradient from the coast to the ocean is lower than it is for ^{228}Ra. Therefore, the activity of ^{228}Ra and the ratio of ^{228}Ra/^{226}Ra are considered useful as tracers of horizontal water mixing (Okubo, 1980; Nozaki et al., 1989; Krest et al., 1999). While the ratios of ^{228}Ra/^{226}Ra at the sea surface have been determined previously in the Pacific Ocean (Moore, 1969; Kaufman et al., 1973; Knauss et al., 1978; Feely et al., 1980; Nozaki et al., 1990), the relative paucity of such data in the northwestern North Pacific and Okhotsk Sea has meant that these data have not been fully utilized to clarify these water mass structures.

This dataset is presented the surface distributions of ^{228}Ra and ^{226}Ra in the northwestern North Pacific and Okhotsk Sea, and will help further understanding of surface water mixing in this region.

2. List of Investigators

Hajime Kawakami (CEIST/JAMSTEC)

3. Sampling and analysis

Samples were collected during the R/V *Mirai* cruises MR00-K01 (Jan.–Feb. 2000) and MR00-K03 (May–Jun. 2000) in the northwestern North Pacific and Okhotsk Sea. Sampling stations and data are shown in Table 1 and Fig. 1. Surface seawater samples were taken using a continuous pumping system, the intake for which is approximately 7 m below the surface. Two kinds of samples were taken at each station, one for the measurement of the isotopic radium ratio, and the other for ^{226}Ra activity. Approximately 200 L of the water from the system was passed through a column (ϕ25 mm 70 mm) packed with manganese-impregnated acrylic fiber (Mn-fiber) at a rate of *ca*. 15 L h^{-1} for concentration of radium isotopes (^{228}Ra and ^{226}Ra). Activity of ^{226}Ra was measured separately by passing 5L of seawater through a column packed with 2 ml of manganese-impregnated acrylic beads (Mn-beads) to concentrate radium (Kawabata et al., 2003). The flow rate of the sample was ca. 14 ml min^{-1}, sufficiently low to bind 100% of the ^{226}Ra onto the Mn-beads (Narita, personal communication). The Mn-fiber and Mn-beads were then taken to a land-based laboratory for the determination of radium.

The Mn-fiber was dissolved with mixture of 2N HCl and H_2O_2 solution. Radium isotopes in the solution were coprecipitated with Ba (Ra) SO_4 and ^{228}Ra/^{226}Ra ratios were determined by γ-spectrometry (Michel et al., 1981; Yamada and Nozaki, 1986). The activities of radium isotopes in the precipitate were measured using a well-type germanium detector (ORTEC GWL-120210). ^{226}Ra activity was estimated from the peaks of its daughters, ^{214}Pb (295 and 352 keV) and ^{214}Bi (609 keV). ^{228}Ra activity was estimated from the peaks of ^{228}Ac at 911 and 964–969 keV. A standard solution of barium (1 mol l^{-1}) was prepared by dissolving low background $Ba(OH)_2 \cdot 8H_2O$ (Strem Chemicals, Inc.) in 1N HCl.

The Mn-beads were also dissolved into the 2N HCl and H_2O_2 mixture, with ^{224}Ra (0.1–0.2 Bq) prepared from ^{228}Th solution using anion-exchange resin (AG1-X8), added as yield tracer. Radium was purified using cation-exchange resin (AG 50W-X12). The solution containing the radium was subsequently heated to dryness. The purified radium

was dissolved with 0.5 ml of 0.05N HCl and 5 ml of 2-propanol, and electroplated onto a stainless-steel planchet (Koide and Bruland, 1975). The planchets were alpha-counted with a silicon surface barrier detector (ORTEC Octete) and the activity of ^{228}Ra was calculated from the ^{228}Ra/^{226}Ra ratio and ^{226}Ra activity.

The salinity at the sea surface was measured using Seacat Thermosalinograph (SBE-21 Sea-Bird Electronics, Inc) onboard the R/V *Mirai*.

4. Dataset

Data obtained from cruises were electronically compiled in an MS Excel file ("228Ra_226Ra_NP.xls"). The data include sampling date, location, salinity, ^{226}Ra activity, ^{228}Ra activity, and acticity ratio of ^{228}Ra relative to ^{226}Ra (^{228}Ra/^{226}Ra). The error in ^{226}Ra, ^{228}Ra, and ^{228}Ra/^{226}Ra measurements was estimated from the counting error.

5. Data analysis

The obtained data was analyzed together with published data (Okubo, 1980; Yamada and Nozaki, 1986; Nozaki et al., 1990; Inoue et al., 2006; Fig. 1).

Evaluation of water mixing in the surface water can be examined in great detail by involving four water masses. Here we seek a fraction (F_n) of a water mass (n) at a station based on the measured parameters, i.e., ^{228}Ra, ^{226}Ra, and salinity. Since F_n is constrained to $0 \leq F_n \leq 1$, the multiple regression analysis is inappropriate in this case. To estimate the mixing ratio of each water mass, we used logistic regression analysis. Equation (1) shows the basic equation of the logistic regression analysis:

$$\ln[P/(1-P)] = \alpha_0 + \alpha_1 X_1 + \alpha_2 X_2 + \alpha_3 X_3 \ldots\ldots\ldots + \alpha_n X_n \qquad (1)$$

where P and α_n are a probability and regression coefficient, respectively, and X's are explanatory variables. Since a fraction, F, of the water masses at a station can be regarded to be equivalent to probability (P) in Equation (1), the logistic equations for the water mass mixing can thus be derived as follows:

$$\ln[F_n/(1-F_n)] = \alpha_{n0} + \alpha_{n1} X_{228} + \alpha_{n2} X_{226} + \alpha_{n3} X_{sal} \qquad (2)$$

where F_n is a fraction of water mass n; n = 1, 2, 3, and 4, representing the four water masses, SAW, OKW, TCW, and the Subtropical Water (STW). X_{228}, X_{226}, and X_{sal} are measured values of ^{228}Ra, ^{226}Ra, and salinity at each station, respectively. Defining the fraction of SAW as a basic category for four subject variables, equation (2) can be arranged as follows:

$$\ln(F_{OKW}/F_{SAW}) = a_0 + a_1 X_{228} + a_2 X_{226} + a_3 X_{sal} \qquad (3)$$

$$\ln(F_{TCW}/F_{SAW}) = b_0 + b_1 X_{228} + b_2 X_{226} + b_3 X_{sal} \qquad (4)$$

$$\ln(F_{STW}/F_{SAW}) = c_0 + c_1X_{228} + c_2X_{226} + c_3X_{sal} \quad (5)$$

In order to evaluate the optimum values for a, b, and c in equations (3–5), initial values of F at each station is required for iterative calculations. Based on previous studies such as that of Yasuda (2003), the stations shown in Fig. 1 were categorized into four groups, each of which was assumed to have 100% of one of four water masses for the first attempt. Finally, calculated values a, b, and c, and measured parameters gives us F_n values. The correlation coefficient (R^2) for the analysis was calculated to be 0.88 ($p < 0.0001$). Note that we did not consider the effect of ^{228}Ra decay, because the time scale for water mixing in this region is relatively shorter than the half-life of ^{228}Ra (5.75y).

The results revealed the distributions of the each water mass in the area studied (Fig. 2). While a high percent of the SAW is observed north of 45°N and east of 160°E in the Subarctic Pacific, its influence extends inside the Okhotsk Sea and further south of the Kuril Islands (Fig. 2a). The southern edge of the 50% SAW contour and the northern edge of the STW almost overlap (green belts of Figs. 2a and b), forming a boundary between the two water masses. The boundary runs northward away from Japan (Fig. 2a and b), a feature that was not revealed by the salinity distribution. In addition, a small but noticeable amount of the STW fraction (ca. 7%) appeared at around 45–50°N, 170°E. This may have been attributed to entrainment of the STW into the Western Subarctic Gyre.

Due to the paucity of data for the Tsugaru Strait, the contribution of the TCW to the Pacific surface water is not well defined at present. Nonetheless, it seems to be confined to the Tsugaru Strait and the coastal region of northern Honshu (Fig. 2c). While the OKW appeared mainly inside the Okhotsk Sea, its influence could be traced further southwestward (Fig. 2d), indicating that the OYW carries the OKW in variable proportions. It was suggested that the mixing of the OKW with SAW resulted in an increase in density which would then lead to these waters descending to a deeper layer (e.g., Yasuda 2003). Consequently, the ratio of the OKW in the surface layer of the Oyashio may decrease as it moves further south. The fractions of TCW at Stn. 1 and

OKW at Stn. 17 were approximately 100% and 6%, respectively (Figs. 4c and d). These features could not be observed in the two end-member mixing results described in Kawakami and Kusakabe (2008). The logistic regression analysis using four end members therefore appears to be more realistic approach with which to estimate water mixing in the northwestern North Pacific.

6. Acknowledgments

We thank the captains, crew, and marine technicians aboard the R/V *Mirai* for their helpful support during these cruises. We are grateful to Ms. S. Hoshi and Ms. T. Nakatani for technical support in the land-based laboratory.

References

Cai, P., Huang, Y., Chen, M., Gou, L., Liu, G., Qiu, Y., 2001. New production based on ^{228}Ra-derived nutrient budgets and thorium-estimated POC export at the intercalibration station in the South China Sea. Deep-Sea Res. I 49, 53–66.

Feely, H., Kipphut, G.W., Trier, R.M., Kent, C., 1980. ^{228}Ra and ^{228}Th in coastal waters. Estuarine Coastal Mar. Sci. 11, 179–205.

Inoue, M., Tanaka, K., Watanabe, S., Kofuji, H., Yamamoto, M., Komura, K., 2006. Seasonal variations of ^{228}Ra/^{226}Ra ratio within coastal waters of the Sea of Japan: implications for water circulation patterns in coastal areas. J. Envrion, Radioact. 89, 138–149.

Kadko, D., Muench, R., 2005. Evaluation of shelf-basin interaction in the western Arctic by use short-lived radium isotopes: The importance of mesoscale processes. Deep-Sea Res. II 52, 3227–3244.

Kawabata, H., Narita, H., Harada, K., Tsunogai, S., Kusakabe, M., 2003. Air-sea gas transfer velocity in stormy winter estimated from radon deficiency. J. Oceanogr. 59, 651–661.

Kaufman, A.A., Trier, R., Broecker, W.S., Feely, H.W., 1973. Distribution of ^{228}Ra in the world ocean. J. Geophys. Res. 78, 8827–8848.

Kawai, H., 1972. Hydrography of the Kuroshio Extension. In: Stommel, H. Yoshida, K. (Eds): Kuroshio: Physical Aspects of the Japan Current. University of Washington Press, Seattle, WA, 235–352.

Kawakami, H., Kusakabe, M., 2008. Surface water mixing estimated from ^{228}Ra and ^{226}Ra in the northwestern North Pacific. J. Environ. Radioact. 99, 1335–1340.

Knauss, K.G., Ku, T.L., Moore, W. S., 1978. Radium and thorium isotopes in the surface waters of east Pacific and coastal southern California. Earth Planet. Sci. Lett. 39, 235–249.

Koide, M., Bruland, K.W. 1975. The electrodeposition and determination of radium by isotopic dilution in sea water and in sedimentssimultaneously with other natural radionuclides. Anal. Chim. Acta 75, 1–19

Krest, J.M., Moore, W.S., Rama, 1999. ^{226}Ra and ^{228}Ra in the mixing zones of the Mississippi and Atchafalaya Rivers: indicators of groundwater input. Mar. Chem. 64, 129–152.

Ku, T.L., Luo, S., Kusakabe, M., Bishop, J.K.B., 1995. ^{228}Ra-derived nutrient budgets in the upper equatorial Pacific and the role of "new" silicate in limiting productivity. Deep-Sea Res. II 42, 479–497.

Legeleux, F., Reyss, J.-L., 1996. ^{228}Ra/^{226}Ra activity ratio in oceanic settling particles: implications regarding the use of barium as a proxy for paleoproductivity reconstruction. Deep-Sea Res. I 43, 1857–1863.

Michel, J., Moore, W.S., King, P.T., 1981. γ-Ray Spectrometry for Determination of Radium-228 and Radium-226 in Natural Waters. Anal. Chem. 53, 1885–1889.

Moore, W.S., 1969. The measurements of ^{228}Ra and ^{228}Th in seawater. J. Geophys. Res. 74, 694–704.

Moore, W.S., Sarmiento, J.L., Key, R.M., 1986. Tracing the Amazon component of surface Atlantic water using ^{228}Ra, salinity and silica. J. Geophys. Res. 91, 2574–2580.

Nakano-Ohta, T., Sato, J., 2006. Determination of ^{228}Ra and ^{226}Ra in seawater collected on manganese-impregnated acrylic fiber. Radioisotopes 55, 443–449.

Nozaki, Y., Yamamoto, Y., 2001. Radium 228 based nitrate fluxes in the eastern Indian Ocean and the South China Sea and a silicon-induced "alkalinity pump" hypothesis. Glob. Biogeochem. Cycles. 15, 555–567.

Nozaki, Y., Kasemsupaya, V., Tsubota, H., 1989. Mean Residence time of the shelf water in the East China and the Yellow seas determined by ^{228}Ra/^{226}Ra measurements. Geophys. Res. Lett. 16, 1297–1300.

Nozaki, Y., Kasemsupaya, V., Tsubota, H., 1990. The distribution of ^{228}Ra and ^{226}Ra in the surface waters of the northern North Pacific. Geochem. J. 24, 1–6.

Ohtani, K., 1989. The role of the Sea of Okhotsk on the Oyashio Water. Umi to Sora 65, 63–83 (in Japanese).

Okubo, T., 1980. Radium-228 in the Japan Sea. J. Oceanogr. Soc. Japan 36, 263–268.

Rutgers van der Loeff, M.M., Key, R. M., Scholten, J., Bauch, D., Michel, A., 1995. ^{228}Ra as a tracer for shelf water in the Arctic Ocean. Deep-Sea Res. II 42, 1533–1553.

Rutgers van der Loeff, M., Kühne, S., Wahsner, M., Höltzen, H., Frank, M., Ekwurzel, B., Mensch, M., Rachold, V., 2003. ^{228}Ra and ^{226}Ra in the Kara and Laptev seas. Continent. Shelf Res. 23, 113–124.

van Beek, P., François, R., Conte,, M. Reyss, J.-L., Souhaut, M. Charette, M., 2007. ^{228}Ra/^{226}Ra and ^{226}Ra/Ba ratios to track barite formation and transport in the water column. Geochim. Cosmochim. Acta 71, 71–86.

Yamada, M., Nozaki, Y., 1986. Radium isotopes in coastal and open surface waters of the western North Pacific. Mar. Chem. 19, 379–389.

Yasuda, I., 2003. Hydrographic Structure and Variability in the Kuroshio-Oyashio Transition Area. J. Oceanogr. 59, 389–402.

Yasuda, I., Okuda, K., Hirai, M., Ogawa, Y., Mizuno, K., Kudoh, H., 1988. Short-term variations of the Tsugaru Warm Current in autumn. Bull. Tohoku Reg. Fish. Lab. 50, 153–191 (in Japanese).

Figure captions

Fig. 1. Sampling locations in the northwestern North Pacific and Okhotsk Sea. Closed and open circles indicate sampling stations of this and previous studies (Okubo, 1980; Yamada and Nozaki, 1986; Nozaki et al., 1990; Inoue et al., 2006), respectively. Numbers adjacent to closed circles correspond to the station numbers in the dataset. Lines with arrow show the ocean currents (Yasuda, 2003).

Fig. 2. Fractions of (a) the western Subarctic Water (SAW), (b) Subtropical Water (STW), (c) Tsugaru Current Water (TCW), and (d) Okhotsk Water (OKW) in the surface layer. The mixing ratios were estimated from logistic regression analysis using ^{226}Ra, ^{228}Ra, and salinity data. Dots indicate sampling locations.

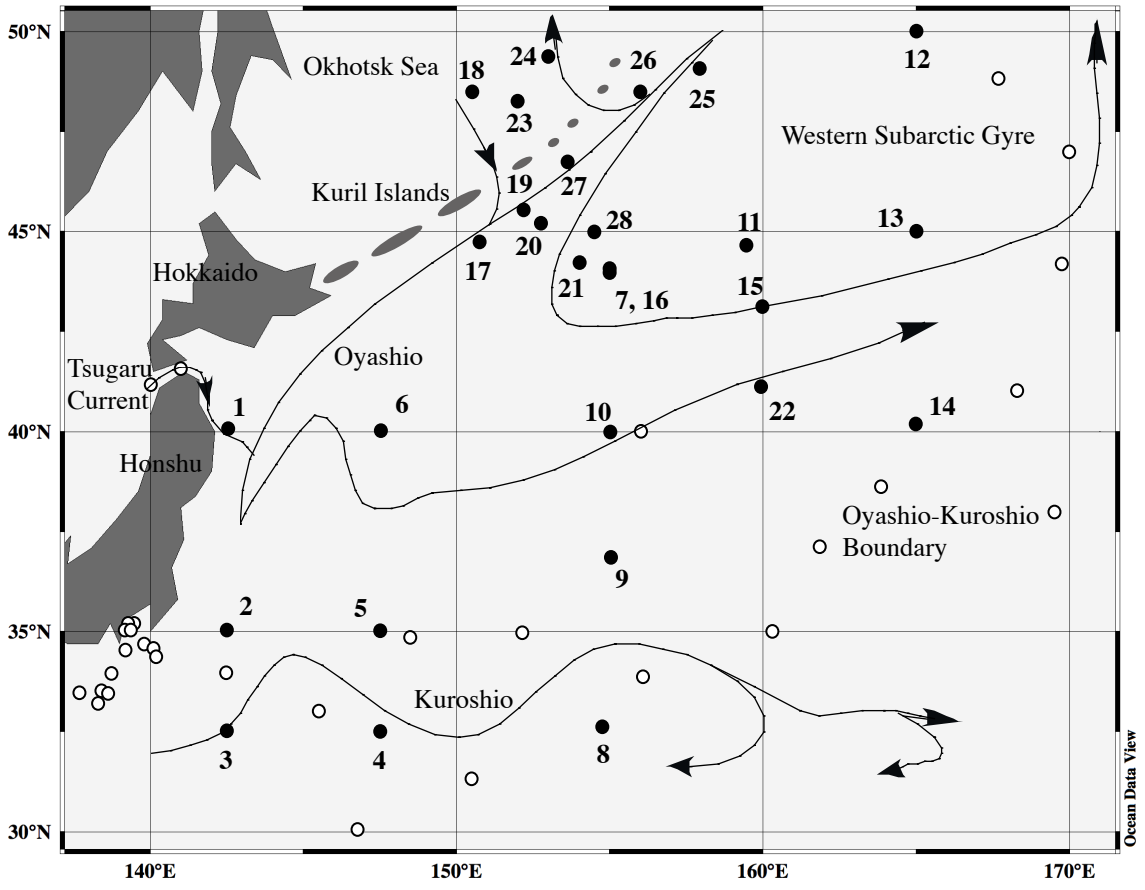
50°N
45°N
40°N
35°N
30°N
140°E
150°E
160°E
170°E
Okhotsk Sea
Kuril Islands
Hokkaido
Tsugaru
Current
Honshu
Oyashio
Western Subarctic Gyre
Oyashio-Kuroshio
Boundary
Kuroshio
1
2
3
4
5
6
7, 16
8
9
10
11
12
13
14
15
17
18
19
20
21
22
23
24
25
26
27
28
Ocean Data View

Fig. 1

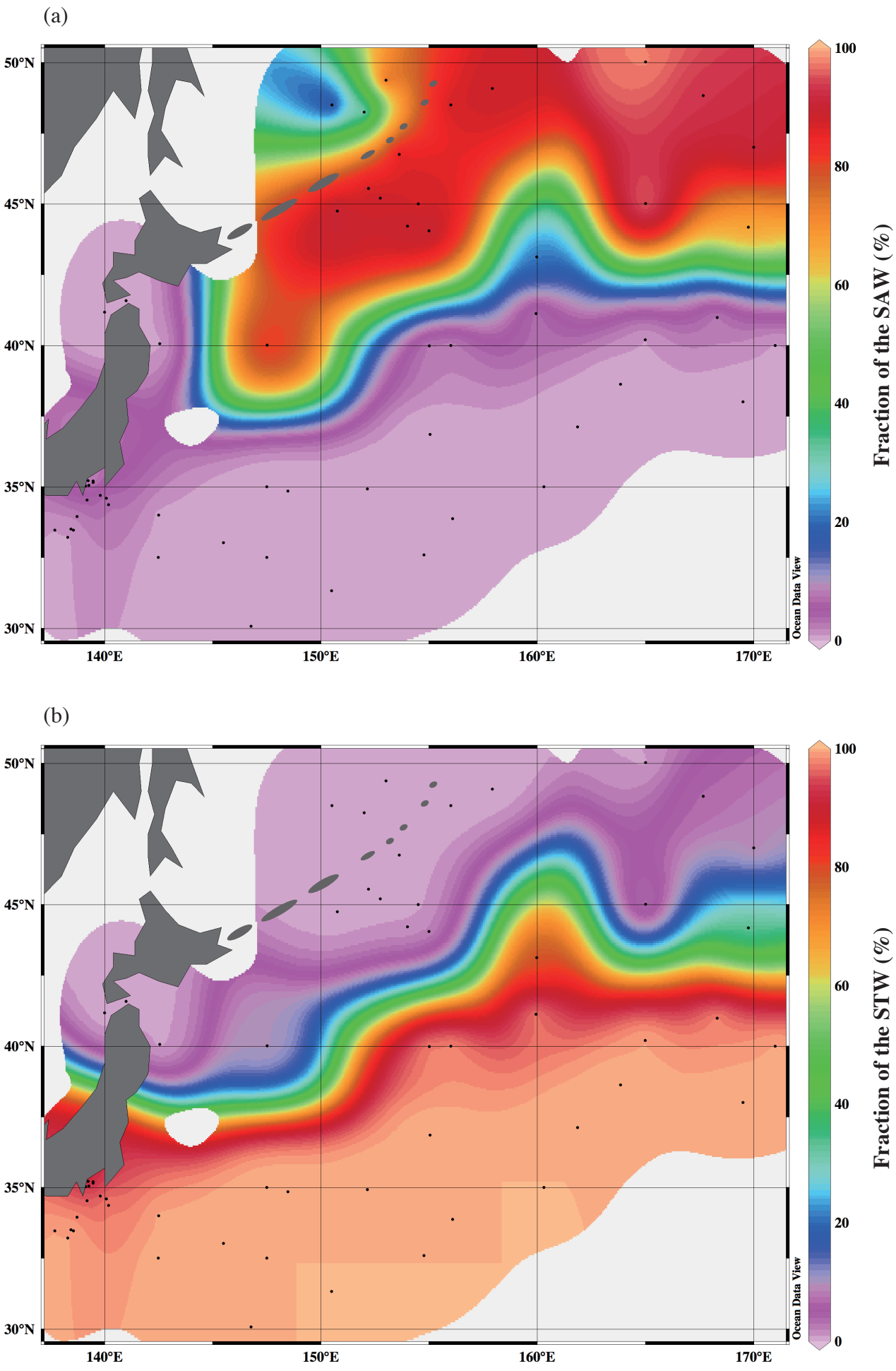
(a)
50°N
45°N
40°N
35°N
30°N
140°E
150°E
160°E
170°E
100
80
60
40
20
0
Fraction of the SAW (%)
Ocean Data View
(b)
50°N
45°N
40°N
35°N
30°N
140°E
150°E
160°E
170°E
100
80
60
40
20
0
Fraction of the STW (%)
Ocean Data View

Fig. 2

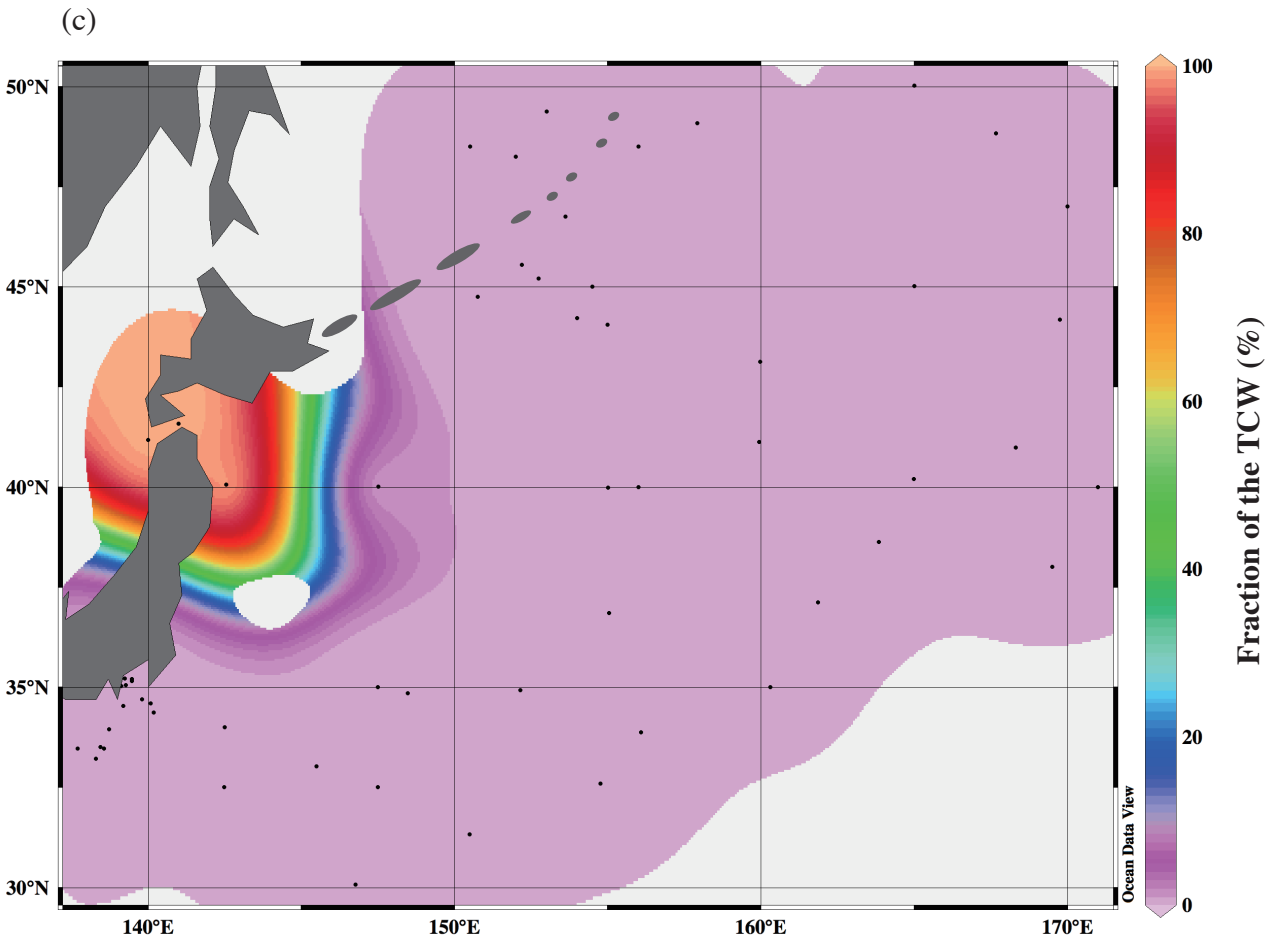

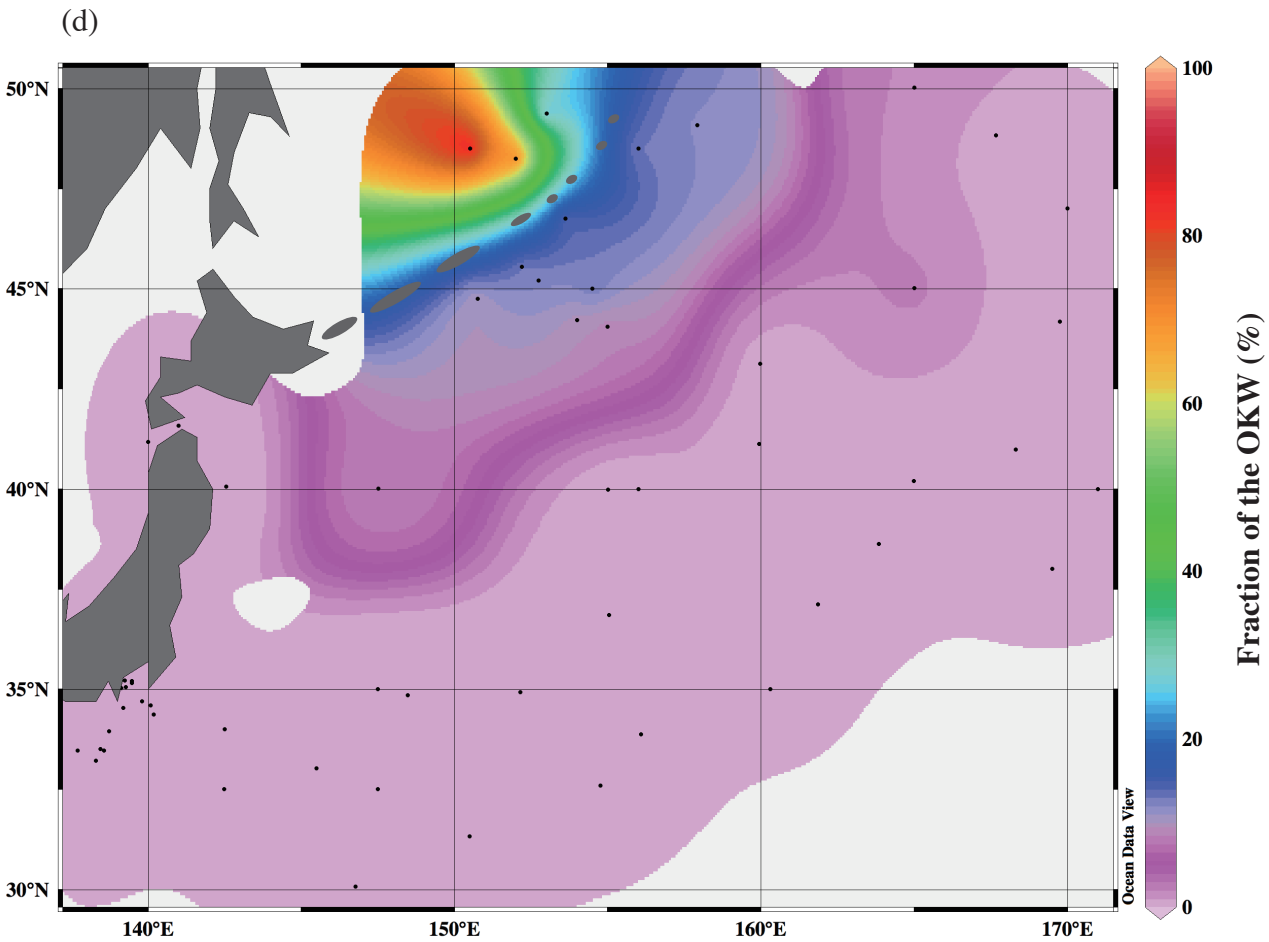

Fig. 2 continued